Graphene Oxide and Polyethyleneimine Cooperative Construct Ionic Imprinted Cellulose Nanocrystals Aerogel for Selective Adsorption of Dy(III)

Xudong Zheng (Zhengks@outlook.com)
Changzhou University https://orcid.org/0000-0003-2688-4855
Wen Sun
Changzhou University
Ang Li
Changzhou University
Bin Wang
Changzhou University
Rong Jiang
Changzhou University
Zhiqiang Song
Changzhou University
Yuzhe Zhang
Changzhou University
Zhongyu Li
Changzhou University

Research Article

Keywords: Cellulose nanocrystals, Aerogel, Graphene oxide, Dysprosium, Adsorption

Posted Date: September 28th, 2021

DOI: https://doi.org/10.21203/rs.3.rs-586534/v2

Version of Record: A version of this preprint was published at Cellulose on November 9th, 2021. See the published version at https://doi.org/10.1007/s10570-021-04299-3.

Abstract

Because of dysprosium's unique physical and chemical properties and limited supply, the price of rare earth dysprosium has been high in recent years. Therefore, the study of the method of high efficiency selective separation of dysprosium has the double value of scientific research and practical economy. In this paper, we used periodic cellulose nanocrystals as the basic structure, polyethylenimine and graphene oxide were introduced, combined with imprinting technology, to construct porous imprinted aerogel and use it for selective adsorption of Dy(III). The physical and chemical properties were characterized by SEM, TEM, FT-IR and TGA. It was proved that both polyethylenimine and graphene oxide were crosslinked effectively with cellulose nanocrystals. Adsorption experiments showed that the composite imprinted aerogel could selectively adsorb dysprosium effectively, and the maximum adsorption capacity for Dy(III) was 36.495 mg g^{-1}. The reproducibility experiment showed that aerogel had good regeneration ability. In conclusion, cellulose nanocrystals aerogel, which is environmentally friendly, efficient and repeatable, is expected to provide a new direction for the recovery of rare earth elements.

1. Introduction

Rare earth elements, known as "industrial vitamins", are widely used in catalysts, permanent magnets, glassmaking, lighting and other fields (Huang and Zhu 2019; Liang et al. 2018; Ni’am et al. 2020; Zhao et al. 2019). Dysprosium (Dy) has always been one of the most important rare earth elements because of its irreplaceable role in optics and permanent magnets (Bisaka et al. 2017; Fujiwara et al. 2016; Liang et al. 2018; Zheng et al. 2020). Moreover,China has attached great importance to the rational development of rare earth resources in recent years. The price of rare earth has changed from "soil" to "rare". Therefore, it is of great significance for sustainable development to explore an economical and green separation and recovery technologies for dysprosium (Kaneko et al. 2019; Prodius et al. 2020).

Since the middle of the 20th century, many scholars have began to pay attention to the processing and recycling of dysprosium ions (Balaram 2019; Habib 2019). In various methods of recovering dysprosium ions, adsorption is an effective alternative because of its simplicity and cost-effectiveness (Kegl et al. 2019). Alcaraz (Alcaraz et al. 2019) synthesized two kinds of activated carbons from waste coffee grounds to adsorb and remove dysprosium ions in aqueous solution. Kaneko (Kaneko et al. 2019) synthesized MPS materials with high selective adsorption properties of dysprosium ions, which provided a new idea for the separation and recovery of dysprosium ions. On the basis of previous studies, we found that the selective adsorption of dysprosium is still a difficult problem because the physical and chemical properties of rare earth elements are directly similar. In addition, the cost of adsorption materials still restricts the industrial application of adsorption process. Therefore, researches on green, low-cost, efficient adsorption materials for selective adsorption of Dy(III) is one of current researching hot directions.

Cellulose nanocrystals (CNCs) are considered as a kind of promising aerogel material due to their green, natural nature and low price (Almeida et al. 2018; Du et al. 2019; Zhang and Zhang 2020). CNCs prepared

by sulfuric acid hydrolysis usually have a diameter of 5–20 nanometers and a length of 10-hundreds of nanometers, and a large number of hydroxyl groups exist on their surfaces (George and S N 2015; Kontturi et al. 2018). Since CNCs can form chiral nematic structures, aerogels made by CNCs have a natural ordered pore structure (Xu et al. 2018), which is conducive to the occurrence of adsorption process (Cao et al. 2020; Kim et al. 2014; Sato et al. 2004). However, the similar properties of other rare earth elements to Dy(III) limit the separation of Dy(III) as a single element, so we introduced imprinting technology (Fang et al. 2021; Zhang et al. 2021) to fix the recognition sites on the surface of CNCs, so as to carry out more effective selective adsorption.

Aerogel has high specific surface area, high porosity and high adsorption capacity, and is one of the materials with the lowest density at present (Du et al. 2013; Salimian et al. 2018), which has been applied in multiple scenarios such as heat insulation materials, storage electrical parts or oil adsorbents, and is a very promising adsorbent material. However, because the colloidal particles in the sol are usually randomly distributed, rapid drying of the gel to aerogel usually produces disordered networks (Long et al. 2018). The technology for preparing ordered aerogels is not well developed. To solve the problem, we introduced ordered CNCs and printed it into aerogels (Xu et al. 2018).

At present, there is not much research on imprinted aerogels, so we aim to introduce imprinting into aerogels and modify them so that the aerogel can adsorb Dy(III) selectively. The branching end of polyethyleneimine (PEI) is rich in primary amine groups, which can easily form crosslinking points with other functional groups, so it is often used in the surface modification of nanomaterials (Zhao et al. 2017). Graphene oxide (GO) has lots of carboxyl, hydroxyl and epoxy groups on its surface, which has the characteristics of a high specific surface area, high strength, good chemical stability and so on (Ashour et al. 2017). As an adsorbent, GO has a high adsorption capacity. Using cellulose nanocrystals as the framework, we prepared a green, imprinted GO-CNCs-PEI aerogel (IGCPA) with a high imprinted adsorption capacity and high selectivity by using ion imprinting technology (Fu et al. 2015) and using GO and PEI as bifunctional monomers to conduct selective adsorption separation of Dy(III) (Jiang et al. 2020; Stepanova et al. 2019), and the cross-linking of GO can also improve the structural strength of the aerogel.

2. Experimental Section

2.1. Materials

Skimmed cotton was bought at a drugstore. Hydrochloric acid (HCl, 37%), Sulfuric acid (H_2SO_4, 98%), Nitric acid (HNO_3, 68%), Glacial acetic acid (CH_3COOH, 99.5%), Sodium hydroxide (NaOH, 96%), 2,2,6,6-Tetramethyl-1-piperidinyloxy (TEMPO, 97%), Ethanol (C_2H_5OH, 99.7%), Sodium bromide (NaBr, 99%) and Sodium hypochlorite (NaClO, Active chlorine ≥ 5.2%) were purchased from Sigma Aldrich. Dysprosium oxide (TREO ≥ 99.9%) was purchased from Shanghai Sinian Metal Materials Co., Ltd. Polyethyleneimine (PEI, 50%), 1-(3-Dimethylaminopropyl)-3-ethylcarbodiimide hydro (EDC, 98%) and N-Hydroxy succinimide (NHS, 98%) were bought from Aladdin Biochemical Technology Co., Ltd. Graphene oxide solutions (GO,

10 mg mL^{-1}) were purchased from Nanjing Xianfeng Nanomaterials Technology Co., Ltd. The dysprosium nitrate ($Dy(NO_3)_3$) used in this study was prepared by dissolving dysprosium oxide with excessive concentrated nitric acid and reheating. The water used in this experiment was distilled water, and all reagents were not further purified unless otherwise specified.

2.2. Instruments

Scanning electron microscope (SEM, JEOL, Japan) was used to observe the surface morphology of the aerogel. The microstructure of the sample was observed using a 300 kV transmission electron microscope (TEM, JEOL 2100, Japan). The samples were tested by a Fourier transform infrared spectrophotometer (FT-IR, IS50, United States). Automatic specific surface and porosity analyzer (BET, ASAP 2460, USA) was used to analyze the specific surface area (S_{BET}) of aerogels. Under N_2 atmosphere, the aerogels were subjected to thermogravimetric analysis using a thermogravimetric analyzer (Q600-TGA/DSC, United States). The concentration of Dy(III) was measured by Inductively coupled plasma atomic emission spectrometer (ICP-OES, Vista-AX, United States).

2.3. Preparation of Samples

The synthesis of CNCs suspension

150 mL H_2SO_4 was added to 150 mL water, stirred evenly and cooled to room temperature. 20 g Skimmed cottons were put into the mixture, stirred it for 2 hours at room temperature, then poured it into 3000 mL ice water, and let it stand for 15 hours for precipitation. The suspension of the lower phase was centrifuged and purified by dialysis until the pH value of the suspension was greater than 2.4.

The synthesis of TEMPO-CNCs suspension

After the CNCs solution (100 mL, 4wt%) was evenly dispersed in 200 mL water, TEMPO (10 mg) and NaBr (100 mg) were added to soak in the solution for 1 hour. Added NaClO solution (40 mL) drop by drop, maintain a pH value of 10.5 with 0.1 M HCl and 0.1 M NaOH, and stirred for 4 hours. Finally, 4 mL C_2H_5OH was added to stop the oxidation reaction. 0.1 M HCl was used to adjust the solution to pH = 7.0. After standing overnight, dialysate was carried out and TEMPO-CNCs suspension was obtained.

The synthesis of PEI-CNCs aerogel

1000 mg PEI (50%) was dispersed in 50 mL TEMPO-CNCs suspension, followed by ultrasonic for 30 minutes, then 250 mg EDC and 250 mg NHS were added into the mixed solution, stirred at room temperature for 24 hours, and dialyzed to obtain a yellow suspension. After freeze drying, PEI-CNCs aerogel was prepared.

The synthesis of GO-CNCs-PEI aerogel (GCPA)

40 mg GO was added to 20 mL PEI-CNCs suspension, the pH value was adjusted to 5.0 with 0.1 M HCl, and the solution was stirred for 3 hours. GCPA was obtained by freeze-drying after dialysis purification.

The synthesis of IGCPA: 40 mg GO and 10 mg $Dy(NO_3)_3$ were added to the 20 mL PEI-CNCs suspension, the pH value was adjusted to 5.0 by 0.1 M HCl and stirred for 3 hours. Freeze drying after dialysis purification. Transferred the aerogel in an eluent (the volume ratio of glacial acetic acid to water is 1:9) for 48 hours to remove Dy(□). Finally, the IGCPA was dried at room temperature after been rinsed three times with ultra-pure water. The preparation process and the possible adsorption mechanism of aerogel are shown in Fig. 1 and Fig. 2.

2.4. Adsorption experiment

Effect of pH on adsorption

$Dy(NO_3)_3$ was used to prepare dysprosium ion original solution with a concentration of 50 mg L^{-1}. We took out 10 mL original solutions and adjusted the pH value to 2.0, 3.0, 4.0, 5.0, 6.0 and 7.0 with 0.1M HCl, respectively. Then we took the solution and placed them in centrifuge tubes. 10 mg adsorbents were then placed in a mixture of solutions in a centrifuge tube and allowed to sit for 24 hours, maintaining the corresponding pH value of the solution. After adsorption was completed, the mixture was centrifuged (10000 r min^{-1}, 15 min) and the absorbents were removed using a 0.22 μm filter. The concentration of Dy(III) in the mixed solution was measured by the ICP-OES at a wavelength of 353.17 nm. The adsorption capacities Q_t (mg g^{-1}) were calculated by the following formula(Mahdi et al. 2018)

$$Q_t = \frac{V\left(C_0 - C_t\right)}{m} \quad (1)$$

Where C_0 and C_t (mg L^{-1}) are initial concentration and the residual concentration of Dy(III) in mixed solution, respectively. V (L) is the volume of Dy(III) stock solution, and m (g) is the mass of aerogel.

Adsorption dynamics: Three Dy(III) original solution (10 mL) was prepared, the pH was adjusted to 5.0, and placed in centrifuge tubes. Three kinds of aerogels (10 mg) were put into the tubes. The concentrations of dysprosium ions in mixed solution were determined at different contact times (0 minutes to 24 hours). We used the software (Origin) to fit the adsorption kinetic data with the pseudo-first-order kinetic model (PFOKM, Eq. (2)) and the pseudo-second-order kinetic model (PSOKM, Eq. (3)) respectively, and then analyzed the adsorption mechanism (Wang et al. 2017).

$$Q_t = Q_e - Q_e e^{-k_1 t} \quad (2)$$

$$Q_t = \frac{k_2 Q_e^2 t}{1 + k_2 Q_e t} \quad (3)$$

Where, Q_t (mg g^{-1}) and Q_e (mg g^{-1}) are the adsorption amount of aerogels at time t and equilibrium, respectively. k_1 (min^{-1}) and k_2 (g mg^{-1} min^{-1}) represent the rate constants of PFOKM and PSOKM, respectively.

Adsorption isotherms: Dy(III) solutions with concentrations of 0,25, 50, 100, 150 and 200 mg L^{-1} were taken, adjusted to pH 5.0, and placed in centrifuge tubes. Three different kinds of aerogels (10 mg) were put into the mixed solutions. The adsorption of Dy(III) by aerogels at different values of initial concentrations was determined 24 hours after the tubes were placed. Langmuir (Eq. (4)) and Freundlich (Eq. (5)) models were used to fit the experimental equilibrium data(Zhu et al. 2018).

$$Q_e = \frac{K_L Q_m C_e}{1 + K_L C_e} \quad (4)$$

$$Q_e = K_F C_e^{1/n} \quad (5)$$

C_e (mg L^{-1}) is the concentration of Dy(III) in solution at equilibrium, Q_m (mg g^{-1}) is the maximum adsorption capacity of aerogels for Dy(III). K_L (L mg^{-1}) is the Langmuir parameter denoted the energy of adsorption and affinity of binding sites. K_F (mg g^{-1}) is the Freundlich sorbent adsorption strength, while $1/n$ is the heterogeneity factors.

Adsorption thermodynamics

10 mg of aerogels were immersed in Dy(□) stock solution (10 mL, pH = 5.0) with different initial concentrations (25, 50, 100 mg L^{-1}). Adsorption tests were carried out at 288.15 K, 298.15 K and 308.15 K, respectively. The residual Dy(III) concentrations in the solution was determined after 24 hours. The values of Gibbs energy (ΔG°) are calculated by equation Eq. (6) (Zhang et al. 2019)

$$\Delta G^{\circ} = -RT \ln K^{\circ} \quad (6)$$

Where thermodynamic equilibrium constant K° is only a function of temperature. It is a constant of dimension 1, in units of "1". It's the vertical intercept of the linear equation of $\ln(C_s/C_e)$ and C_s. Wherein, C_s (mmol g^{-1}) is the adsorption amount per gram of aerogels, and C_e is the concentration of Dy(III) in the mixed solution at adsorption equilibrium. R (8.314 J mol^{-1} K^{-1}) is the universal gas constant, and T is the given temperature. Eventually, entropy (ΔS°) and the enthalpy (ΔH°) values are obtained from van't Hoff equation Eq. (7) (Zheng et al. 2020):

$$\ln K^{\circ} = \frac{\Delta S}{R} - \frac{\Delta H}{RT} \quad (7)$$

Selective tests: 10 mg aerogels were immersed in 10 mL mixed solution with coexisting system (Dy(III), Nd(III) and Pr(III) were provided by $Dy(NO_3)_3$, $Nd(NO_3)_3$ and $Pr(NO_3)_3$ respectively). The initial concentration of each cation was 50 mg L^{-1}, and the pH value was adjusted to 5.0 with 0.1M HCl. The concentration in the mixed solution was measured 24 hours after the tubes were placed at 25°C. The selectivity of aerogels was evaluated by K_d (mL g^{-1}). Relationships are listed as follow (Eq. (8)) (Sun et al. 2017):

$$K_d = \frac{V\left(C_0 - C_f\right)}{mC_f} \quad (8)$$

Where, C_0 and C_f are initial and final concentration of each rare earth ion, respectively. The C_0 of each cation is 50 mg L^{-1}.

Reusability tests: After each adsorption process, the aerogels were separated from the solution by elution (10% glacial acetic acid solution) for 24 hours to remove the adsorbed Dy(III). These aerogels are then reused for adsorption experiments. We took stock solutions (50 mg L^{-1}), adjusted the pH to 5.0, and placed in a centrifuge tube. The adsorbents were then put into the solution. The residual concentration of Dy(III) in the solution was determined after 24 hours at 25℃. The whole adsorption-desorption experiment was repeated 5 times. The reusability of the aerogels was verified by the changes of five adsorption capacities of the aerogels.

3. Results And Discussion

3.1. Aerogel characterization

SEM analysis

The microstructure and surface morphology of composite aerogels were observed by scanning electron microscopy (SEM), as shown in Fig. 3. Under the combined action of GO and PEI, the materials showed the good porous structure. It can be seen that the material is composed of a large number of pores, which contributes to the ultra-light performance of the aerogels and also provides lots of adsorption sites for Dy(III) adsorption. The pores on the surface of PEI-CNCS aerogels, GCPA and IGCPA all have good periodicity, indicating that the composite aerogels can effectively replicate the structure of CNCs, the subsequent modification and the elution of imprinted ions have no effect on the structure of aerogels, which effectively maintain the periodicity template of the materials. In addition, in Fig. 3 (b) and Fig. 3 (c), PEI and GO are uniformly distributed on the porous network of CNCs, indicating that the cross-linking between PEI and GO and CNCs is stable. The adhesion of GO to CNCs not only added additional adsorption sites, but also prevented the agglomeration of CNCs to a certain extent, which contributed to the efficient adsorption of Dy(III) by the adsorbent.

TEM analysis

TEM images (Fig. 4) shows that the three aerogels all exhibit uniformly arranged pore structures, which match the size in SEM images, confirming the successful preservation of periodic structures. Compared with PEI-CNCs, GCPA and IGCPA increased the flake morphology of GO, indicating that GO can successfully adhere to CNCs and maintain the original structure. Compared with non-imprinted aerogels, the eluted imprinted aerogels also have better pore structure and show good stability. All these are consistent with the SEM results mentioned above. In addition, the elemental composition of IGCPA was

analyzed by EDS, as shown in Fig. 4 (d). The elemental analysis results are consistent with the expected C, N, and O elements. The cross-linking reaction of PEI increased the intensity of N signal, and dysprosium was not detected, which further confirmed that the cross-linking reaction was an effective method for preparing amine-rich porous aerogels.

BET analysis

The N_2 adsorption-desorption analysis isotherm was shown in Fig. 5 and Table 1. It can be seen from the isotherm fitting curve that the three kinds of aerogels adsorption processes all belong to type IV. When the relative pressure is in the low-pressure region (0.0-0.3 P/P_0), the upward curve is a monolayer adsorption process. When the monolayer adsorption reaches saturation, the multilayer adsorption begins. As the pressure increases, the pore size of the aggregate expands, resulting in the subsequent phenomenon. The curves of adsorption return line adsorption and desorption formed are very steep, and the relative pressure of condensation and evaporation is in the middle. Therefore, the surface of IGCPA is a cylindrical hole with openings at both ends, which is consistent with the results of SEM images. In addition, the S_{BET} of PEI-CNC, GCPA and IGCPA were 4.175, 10.832 and 14.372 $m^2\ g^{-1}$, respectively. With the further functionalization of CNCs by PEI and GO, the S_{BET} of the material increased and the pore size became smaller, this may be due to the new pores generated on the surface of the CNCs. The small pores in the eluted IGCPA collapsed to form large pores, which caused the S_{BET} of the aerogel to become larger and the pore size also increased. In addition, the specific surface area of composite aerogels is generally smaller, most likely due to the formation of large aggregates or aggregates during drying (Brinkmann et al. 2016; Peng et al. 2011; Zheng et al. 2020).

Table 1
The pore structure parameters of four aerogels.

Sample	Surface Area (cm^2/g)	Pore Size (nm)
PEI-CNCs	4.1750	24.836
GCPA	10.832	12.589
IGCPA	14.372	19.779

FT-IR analysis: Infrared spectra were measured, and FT-IR spectra of TEMPO-CNCs after freeze drying and three aerogels were shown in Fig. 6. It is worth noting that the spectrum of TEMPO-CNCs have a strong peak at 1627 cm^{-1}, which is a characteristic peak of the carbonyl of the carboxylic acid groups. There were three strong peaks in PEI-CNCs spectrum at 1644, 1567 and 1461 cm^{-1}, indicating the characteristic peaks of amide bond and an amino group. In addition, PEI-CNCs showed a strong spectral band in the range of 3100–3550 cm^{-1}, which was due to the stretching vibration of O-H and N-H at 3100–3500 cm^{-1}. Therefore, it can be proved that the amino group has been successfully introduced in the cross-linking process of PEI. The peaks of GCPA and IGCPA at 2904 cm^{-1} were observed to change, which was attributed to the stretching vibration of $-CH_2$ due to defects in the graphite structure. It can be

concluded that GO was successfully introduced into GCPA and IGCPA. In addition, the peaks of eluted IGCPA were consistent with that of GCPA, indicating that imprinted ions in IGCPA were completely washed and other groups remained stable, which proved that the modified material had good stability.

TG/DTG analysis

The thermal stability of the material was investigated by increasing the temperature from 30℃ to 800℃ in N_2 atmosphere. The thermogravimetric results are shown in Fig. 7. When the temperature reaches 250℃, decomposition is obvious and the mass decreases by 15–25%, which is mainly due to water loss. The total mass loss between 250–400℃ can be explained by the decomposition of the nanofiber network structure. Above 400℃, entering the final carbonization stage, the mass loss gradually stops, the TGA curve flattens out, and the residue is mainly composed of carbon left by calcination. The above results show that the addition of GO, PEI and other materials improves the thermal stability of the materials. The total mass loss rate of IGCPA was less than that of GCPA, indicating that the imprinted aerogels had better thermal stability.

3.2. Analysis of adsorption results

Effect of pH on adsorption

The pH value affects the presence of cations in the solution and the surface charge of the adsorbent. In order to avoid Dy^{3+} from forming dysprosium hydroxide precipitation under alkaline conditions, the adsorption properties in the pH range of 2.0–7.0 were studied. As can be seen from Fig. 8, with the increase of pH value, the adsorption amount of each adsorbent gradually increases. The adsorption capacity increased rapidly in the pH 1.0–5.0 range. When the pH value was higher than 5.0, the adsorption capacity gradually stabilized, which could be attributed to the low degree of dissociation of the -COOH group. In addition, the adsorption capacity of non-imprinted aerogels is much lower than that of non-imprinted aerogels. The imprinted factor (IF) defines the adsorption capacity ratio of imprinted and non-imprinted aerogels and shows the separation capacity of the aerogels. When pH = 5.0, the maximum value is 1.420, and the imprinted aerogel can achieve the highest adsorption capacity. Therefore, in subsequent adsorption experiments, we set the pH = 5.0.

Adsorption dynamics

The relationship between the adsorption quantity (Q_t) and contact time (t) was discussed by adsorption dynamics experiments. As can be seen from Fig. 9, the adsorption curve of aerogels grew rapidly at the beginning and reached 80% of the maximum adsorption capacity within 200 minutes. Then, the adsorption curve grew slowly and finally reached an adsorption equilibrium within 6 hours, at which time the blot sites on the aerogels became saturated. The adsorption capacity of GCPA and IGCPA introduced with GO was significantly higher than that of PEI-CNCs, and IGCPA had higher adsorption equilibrium than GCPA due to its unique imprinted hole. The PFOKM and PSOKM were fit the kinetic data to investigate the adsorption rate constant and adsorption mechanism. The relevant calculation parameters

of the adsorption kinetics model are shown in Table 2. Obviously, the PSOKM model ($R^2 \geq 0.990$) and the kinetic data fit well, indicating that the main adsorption process is chemical adsorption.

Table 2
Kinetic constants for the Pseudo-first-order and Pseudo-second-order models.

Sorbents	Pseudo-first-order kinetic model			Pseudo-second-order kinetic model		
	Q_e (mg g^{-1})	$k_1 \times 10^{-2}$ (min^{-1})	R^2	Q_e (mg g^{-1})	$k_2 \times 10^{-2}$ (g mg^{-1} min^{-1})	R^2
PEI-CNCs	15.429	2.809	0.981	16.372	0.250	0.993
GCPA	25.878	3.357	0.970	27.391	0.179	0.990
IGCPA	33.771	3.760	0.984	35.601	0.157	0.990

Adsorption isotherm: By contacting Dy(III) solution with different initial concentration (0-200 mg L^{-1}), the differences of Dy(III) adsorption by different aerogels were analyzed, as well as the equilibrium data and adsorption curves. Langmuir isothermal model and Freundlich isothermal model were used to fit the experimental data of aerogels. As shown in Fig. 10, the adsorption capacity increased synchronously with the increase of the initial Dy(III) concentration. The maximum adsorption capacities of GCPA and IGCPA were 26.678 and 36.495 mg g^{-1}, respectively. Its high adsorption capacity was attributed to the functionalization of CNCs by GO and PEI, which provided more binding sites for Dy(III). Table 3 summarizes the relevant isothermal constants. The larger R^2 value (0.991–0.999) indicated that the Langmuir isothermal adsorption model could fit the experimental data well, and the adsorption process by aerogels proved to be monolayer adsorption. The lower value of $1/n$ indicates that IGCPA has better adsorption conditions for Dy(III) than GCPA.

Table 3
Adsorption equilibrium constants for Langmuir and Freundlich isotherm equations.

Sorbents	Langmuir			Freundlich		
	Q_m (mg g^{-1})	K_L (L mg^{-1})	R^2	K_F (mg g^{-1})	$1/n$	R^2
PEI-CNCs	18.972	0.0869	0.999	6.157	0.217	0.894
GCPA	26.678	0.119	0.991	10.243	0.188	0.871
IGCPA	36.495	0.397	0.994	22.557	0.100	0.744

Adsorption thermodynamics: The effects of three kinds of aerogels on the adsorption at different temperatures (288.15 K, 298.15 K and 308.15 K) were studied. ΔG° was calculated according to the Gibb's free energy change equation (Fig. 11), and ΔH° and ΔS° are obtained by the relation between $\ln K^\circ$ and $1/T$ (Fig. 12). Table 4 lists three aerogels thermodynamics related parameters. ΔG° is negative between − 5.363 and − 6.742 kJ mol^{-1}, indicating that the adsorption of Dy(III) is spontaneous, and the higher the

temperature, the more favorable the adsorption process. ΔH° is positive, indicating that the adsorption process is endothermic, which proves again that the increase of temperature is conducive to adsorption. ΔS° is positive, indicating that the adsorption process is an entropy increase process. In summary, the adsorption of Dy(III) by aerogels is spontaneous, endothermic and entropy-enhancing.

Table 4
Thermodynamic parameters of three aerogels.

Sorbents	ΔH° (kJ mol^{-1})	ΔS° (J mol^{-1})	T (K)	K°	ΔG° (kJ mol^{-1})	R^2
PEI-CNCs	4.011	32.547	288.15	9.382	-5.363	0.993
			298.15	9.979	-5.702	
			308.15	10.457	-6.014	
GCPA	4.313	35.023	288.15	11.188	-5.785	0.990
			298.15	11.789	-6.116	
			308.15	12.577	-6.487	
IGCPA	5.228	38.869	288.15	12.064	-5.966	0.991
			298.15	13.086	-6.374	
			308.15	13.897	-6.742	

Selective tests: In order to prove that IGCPA has good adsorption selectivity, a competitive adsorption experiment was carried out. The aerogels adsorbed Dy(III) as well as Pr(III) and Nd(III). The result is shown in Fig. 13 and Table 5. The K_d value reflects adsorption selectivity of adsorbents for Dy(III). The K_d value of IGCPA for Dy(III) is higher than that of GCPA, the maximum K_d value is 1909.2 mL g^{-1} of IGCPA. It can be seen that the unique imprinted hole on IGCPA has a specific adsorption on Dy(III), and this site cannot adsorb other rare earth ions. Compared with other adsorption experiments, the total adsorption capacity of IGCPA for the three rare earth ions is higher than that of single dysprosium ion, which indicates that IGCPA can also adsorb Nd(III) and Pr(III). In this experiment, the adsorption capacity of IGCPA for Dy(III) decreased, indicating that other rare earth ions would interfere with the adsorption of Dy(III). According to Pearson's law, this is because Dy(III), Nd(III) and Pr(III) are all hard Lewis acids, and the strongest ion competition often occurs between the same type of metals. In addition, the results show that the order of adsorption capacity is Dy(III) > Nd(III) > Pr(III). We speculate that this is related to the ion radius. The smaller the radius, the stronger the chelating ability of the metal ion to the carboxyl group. In summary, IGCPA can preferentially separate Dy(III) from the multi-ion coexistence system.

Table 5
The K_d value of Dy(III) adsorbed by aerogels in mixed solution.

Cation	PEI-CNCs		GCPA		IGCPA	
	C_f (mg L^{-1})	K_d (mL g^{-1})	C_f (mg L^{-1})	K_d (mL g^{-1})	C_f (mg L^{-1})	K_d (mL g^{-1})
Pr(III)	35.874	393.77	31.707	597.09	31.718	576.39
Nd(III)	35.779	397.47	31.121	606.63	31.379	593.42
Dy(III)	35.456	410.20	31.003	612.75	17.187	1909.2

Regeneration: The reuse of adsorbents will minimize industrial production costs. As can be seen from Fig. 14, five adsorption cycles were performed to test the reliability of the aerogel. After 5 cycles, the adsorption capacity decreased to 67.97–79.75% of the initial adsorption capacity, which was mainly due to the loss of adsorption sites caused by eluent elution, and the SEM image of IGCPA was basically the same as before the test. In conclusion, IGCPA has reliable repeatability and is expected to be a commercially available adsorption material. Further, some other adsorbents are listed to compare adsorption capacities for REEs in Table 6 (Zhao et al. 2017; Zheng et al. 2016; Zheng et al. 2019; Zheng et al. 2020).

Table 6
Comparison of IGCPA with those described in other literature

Sorbents	Cation	pH	Adsorption capacity (mg g^{-1})	References
IGCPA	Dy(III)	5.0	36.495	This study
o-CNCs/GO-IIPs	Dy(III)	4.0	41.790	(Zheng et al. 2020)
Imprinted mesoporous silica materials	Dy(III)	2.0	22.330	(Zheng et al. 2016)
Imprinted mesoporous cellulose films	Nd(III)	4.0	22.610	(Zheng et al. 2019)
PEI-cross-linked CNC (PEI-CNC)	Er(III)	5.4	120.29	(Zhao et al. 2017)

4. Conclusions

In this study, under the circumstance of environmental pollution caused by rare earth elements and the urgent need to reduce the cost, the imprinted aerogel IGCPA with periodic structure was prepared from biodegradable cellulose nanocrystals and used for the specific adsorption of Dy(III) in rare earth waste. GO and PEI were uniformly distributed on the CNCs skeleton and did not affect the crystallization zone. The carboxyl group introduced by surface modification further improved the adsorption capacity of Dy(III) as a synergistic functional monomer. The results showed that the optimum pH value for adsorption was

5.0. PSOKM can fit the adsorption data well, indicating that aerogel adsorption of Dy(III) is mainly a chemical process. According to the adsorption isotherm, the adsorption process was mainly monolayer adsorption, and the maximum adsorption capacity was 36.495 mg g^{-1}. In multi-ion coexisting systems, imprinted aerogels tend to adsorb Dy(III). In addition, the repeated use test shows that the material has strong regeneration performance. The results show that the composite imprinted aerogel can adsorb Dy(III) efficiently and greenly.

Declarations

Acknowledgement

The authors thank the National Natural Science Foundation of China (Grant Nos. 21876015, 21808018, 21878026, 22008014), Postgraduate Research & Practice Innovation Program of Jiangsu Province (No. KYCX20_2579, No. KYCX20_2592 and No. KYCX20_2595). Also, the author would like to thank the researchers at the Analytical Testing Center of Changzhou University for their assistance in SEM, FTIR and TG analysis.

Conflict of interest

The authors declare that they have no conflict of interest.

Ethical approval

The article does not contain any experiments with human participants or animals performed by any of the authors.

Informed consent

Informed consent was obtained from all individual participants included in the study.

References

1. Alcaraz L, Escudero ME, Alguacil FJ, Llorente I, Urbieta A, Fernández P, López FA (2019) Dysprosium Removal from Water Using Active Carbons Obtained from Spent Coffee Ground Nanomaterials 9 doi:10.3390/nano9101372
2. Almeida APC, Canejo JP, Fernandes SN, Echeverria C, Almeida PL, Godinho MH (2018) Cellulose-Based Biomimetics and Their Applications Advanced Materials 30 doi:10.1002/adma.201703655
3. Ashour RM et al. (2017) Rare Earth Ions Adsorption onto Graphene Oxide Nanosheets Solvent Extraction and Ion Exchange 35:91-103 doi:10.1080/07366299.2017.1287509
4. Balaram V (2019) Rare earth elements: A review of applications, occurrence, exploration, analysis, recycling, and environmental impact Geoscience Frontiers 4: 1285-1303 doi:10.1016/j.gsf.2018.12.005

5. Bisaka K, Thobadi IC, Pawlik C (2017) Extraction of rare earths from iron-rich rare earth deposits J S Afr Inst Min Metall 117:731-739 doi:10.17159/2411-9717/2017/v117n8a2
6. Brinkmann A, Chen M, Couillard M, Jakubek ZJ, Leng T, Johnston LJ (2016) Correlating Cellulose Nanocrystal Particle Size and Surface Area Langmuir 32:6105-6114 doi:10.1021/acs.langmuir.6b01376
7. Cao Y, Wang PX, D'Acierno F, Hamad WY, Michal CA, MacLachlan MJ (2020) Tunable Diffraction Gratings from Biosourced Lyotropic Liquid Crystals Advanced Materials 32 doi:10.1002/adma.201907376
8. Du A, Zhou B, Zhang Z, Shen J (2013) A Special Material or a New State of Matter: A Review and Reconsideration of the Aerogel Materials 6:941-968 doi:10.3390/ma6030941
9. Du H, Liu W, Zhang M, Si C, Zhang X, Li B (2019) Cellulose nanocrystals and cellulose nanofibrils based hydrogels for biomedical applications Carbohydrate Polymers 209:130-144 doi:10.1016/j.carbpol.2019.01.020
10. Fang L, Miao Y, Wei D, Zhang Y, Zhou Y (2021) Efficient removal of norfloxacin in water using magnetic molecularly imprinted polymer Chemosphere 262:128032 doi:10.1016/j.chemosphere.2020.128032
11. Fu J, Chen L, Li J, Zhang Z (2015) Current status and challenges of ion imprinting Journal of Materials Chemistry A 3:13598-13627 doi:10.1039/c5ta02421h
12. Fujiwara I, Takeuchi K, Murakami Y (2016) Development of a Dysprosium (III) Ion-selective Electrode Using a Dysprosium (III)-imprinted Polymer Bunseki Kagaku 65:527-531 doi:10.2116/bunsekikagaku.65.527
13. George J, S N S (2015) Cellulose nanocrystals: synthesis, functional properties, and applications Nanotechnology, Science and Applications doi:10.2147/nsa.S64386
14. Habib K (2019) A products classification approach to optimize circularity of critical resources-the case of NdFeB magnets Journal of Cleaner Production:90-97 doi:10.1016/j.jclepro.2019.05.048
15. Huang H, Zhu JJ (2019) The electrochemical applications of rare earth-based nanomaterials Analyst 144:6789-6811 doi:10.1039/c9an01562k
16. Jiang W, Shen P, Yi J, Li L, Wu C, Gu J (2020) Surface modification of nanocrystalline cellulose and its application in natural rubber composites Journal of Applied Polymer Science 137 doi:10.1002/app.49163
17. Kaneko T, Hikosaka R, Nagata F, Inagaki M, Kato K (2019) Effective adsorption of dysprosium ions on amino and carboxyl functionalized mesoporous silica sheets J Asian Ceram Soc 7:213-220 doi:10.1080/21870764.2019.1606139
18. Kegl T, Ban I, Lobnik A, Košak A (2019) Synthesis and characterization of novel γ-Fe2O3-NH4OH@SiO2(APTMS) nanoparticles for dysprosium adsorption Journal of Hazardous Materials 378 doi:10.1016/j.jhazmat.2019.120764
19. Kim J, Sadasivuni KK, Zhai L, Gao X, Jo EB (2014) Cellulose Nanocrystals and Nanofibers for Smart Optics Materials. Paper presented at the 2014 International Symposium on Optomechatronic

Technologies,

20. Kontturi E, Laaksonen P, Linder MB, Nonappa, Groschel AH, Rojas OJ, Ikkala O (2018) Advanced Materials through Assembly of Nanocelluloses Adv Mater 30:e1703779 doi:10.1002/adma.201703779
21. Liang XD, Ye M, Yang L, Fu WB, Li Z (2018) Evaluation and Policy Research on the Sustainable Development of China's Rare Earth Resources Sustainability 10:16 doi:10.3390/su10103792
22. Long L-Y, Weng Y-X, Wang Y-Z (2018) Cellulose Aerogels: Synthesis, Applications, and Prospects Polymers 10 doi:10.3390/polym10060623
23. Mahdi Z, Yu QJ, El Hanandeh A (2018) Competitive adsorption of heavy metal ions (Pb^{2+}, Cu^{2+}, and Ni^{2+}) onto date seed biochar: batch and fixed bed experiments Separation Science and Technology 54:888-901 doi:10.1080/01496395.2018.1523192
24. Ni'am AC, Wang Y-F, Chen S-W, Chang G-M, You S-J (2020) Simultaneous recovery of rare earth elements from waste permanent magnets (WPMs) leach liquor by solvent extraction and hollow fiber supported liquid membrane Chemical Engineering and Processing - Process Intensification 148 doi:10.1016/j.cep.2020.107831
25. Peng Y, Gardner DJ, Han Y (2011) Drying cellulose nanofibrils: in search of a suitable method Cellulose 19:91-102 doi:10.1007/s10570-011-9630-z
26. Prodius D, Gandha K, Mudring AV, Nlebedim IC (2020) Sustainable Urban Mining of Critical Elements from Magnet and Electronic Wastes ACS Sustain Chem Eng 8:1455-1463 doi:10.1021/acssuschemeng.9b05741
27. Salimian S, Zadhoush A, Naeimirad M, Kotek R, Ramakrishna S (2018) A review on aerogel: 3D nanoporous structured fillers in polymer-based nanocomposites Polym Compos 39:3383-3408 doi:10.1002/pc.24412
28. Sato K, Mochizuki H, Okajima K, Yamane C (2004) Effects of Hydrophobic Solvents on X-Ray Diffraction Patterns of Regenerated Cellulose Membrane Polymer Journal 36:478-482 doi:10.1295/polymj.36.478
29. Stepanova M, Averianov I, Gofman I, Solomakha O, Nashchekina Y, Korzhikov-Vlakh V, Korzhikova-Vlakh E (2019) Poly(ε-caprolactone)-based biocomposites reinforced with nanocrystalline cellulose grafted with poly(L-lactic acid) IOP Conference Series: Materials Science and Engineering 500 doi:10.1088/1757-899x/500/1/012021
30. Sun D, Zhu Y, Meng M, Qiao Y, Yan Y, Li C (2017) Fabrication of highly selective ion imprinted macroporous membranes with crown ether for targeted separation of lithium ion Sep Purif Technol 175:19-26 doi:10.1016/j.seppur.2016.11.029
31. Wang L, Zhao X, Zhang J, Xiong Z (2017) Selective adsorption of Pb (II) over the zinc-based MOFs in aqueous solution-kinetics, isotherms, and the ion exchange mechanism Environmental Science and Pollution Research 24:14198-14206 doi:10.1007/s11356-017-9002-9
32. Xu Y, Dai Y, Nguyen T, Hamad WY, MacLachlan MJ (2018) Aerogel materials with periodic structures imprinted with cellulose nanocrystals Nanoscale 10:3805-3812 doi:10.1039/c7nr07719j

33. Zhang J, Zhang J (2020) Advanced functional materials based on cellulose Acta Polymerica sinica:1376-1398
34. Zhang L, Li L, Shi D, Peng X, Song F, Nie F (2019) Kinetics and mechanism study of lithium extraction from alkaline solution by HFTA and TOPO and stripping process using Lewis cell technique Sep Purif Technol 211:917-924 doi:10.1016/j.seppur.2018.10.043
35. Zhang Y, Bian T, Jiang R, Zhang Y, Zheng X, Li Z (2021) Bionic chitosan-carbon imprinted aerogel for high selective recovery of Gd() from end-of-life rare earth productions J Hazard Mater 407:124347 doi:10.1016/j.jhazmat.2020.124347
36. Zhao F et al. (2017) Polyethylenimine-cross-linked cellulose nanocrystals for highly efficient recovery of rare earth elements from water and a mechanism study Green Chemistry 19:4816-4828 doi:10.1039/c7gc01770g
37. Zhao H, Xia J, Yin D, Luo M, Yan C, Du Y (2019) Rare earth incorporated electrode materials for advanced energy storage Coordination Chemistry Reviews 390:32-49 doi:10.1016/j.ccr.2019.03.011
38. Zheng X, Liu E, Zhang F, Yan Y, Pan J (2016) Efficient adsorption and separation of dysprosium from NdFeB magnets in an acidic system by ion imprinted mesoporous silica sealed in a dialysis bag Green Chemistry 18:5031-5040 doi:10.1039/c6gc01426g
39. Zheng X, Zhang Y, Bian T, Wang D, Li Z (2019) One-step fabrication of imprinted mesoporous cellulose nanocrystals films for selective separation and recovery of Nd(III) Cellulose 26:5571-5582 doi:10.1007/s10570-019-02482-1
40. Zheng XD, Zhang Y, Bian TT, Zhang YZ, Li ZY, Pan JM (2020) Oxidized carbon materials cooperative construct ionic imprinted cellulose nanocrystals films for efficient adsorption of Dy(III) Chem Eng J 381:10 doi:10.1016/j.cej.2019.122669
41. Zhu Y, Niu Y, Li H, Ren B, Qu R, Chen H, Zhang Y (2018) Removal of Cd(II) and Fe(III) from DMSO by silica gel supported PAMAM dendrimers: Equilibrium, thermodynamics, kinetics and mechanism Ecotoxicol Environ Saf 162:253-260 doi:10.1016/j.ecoenv.2018.06.094

Figures

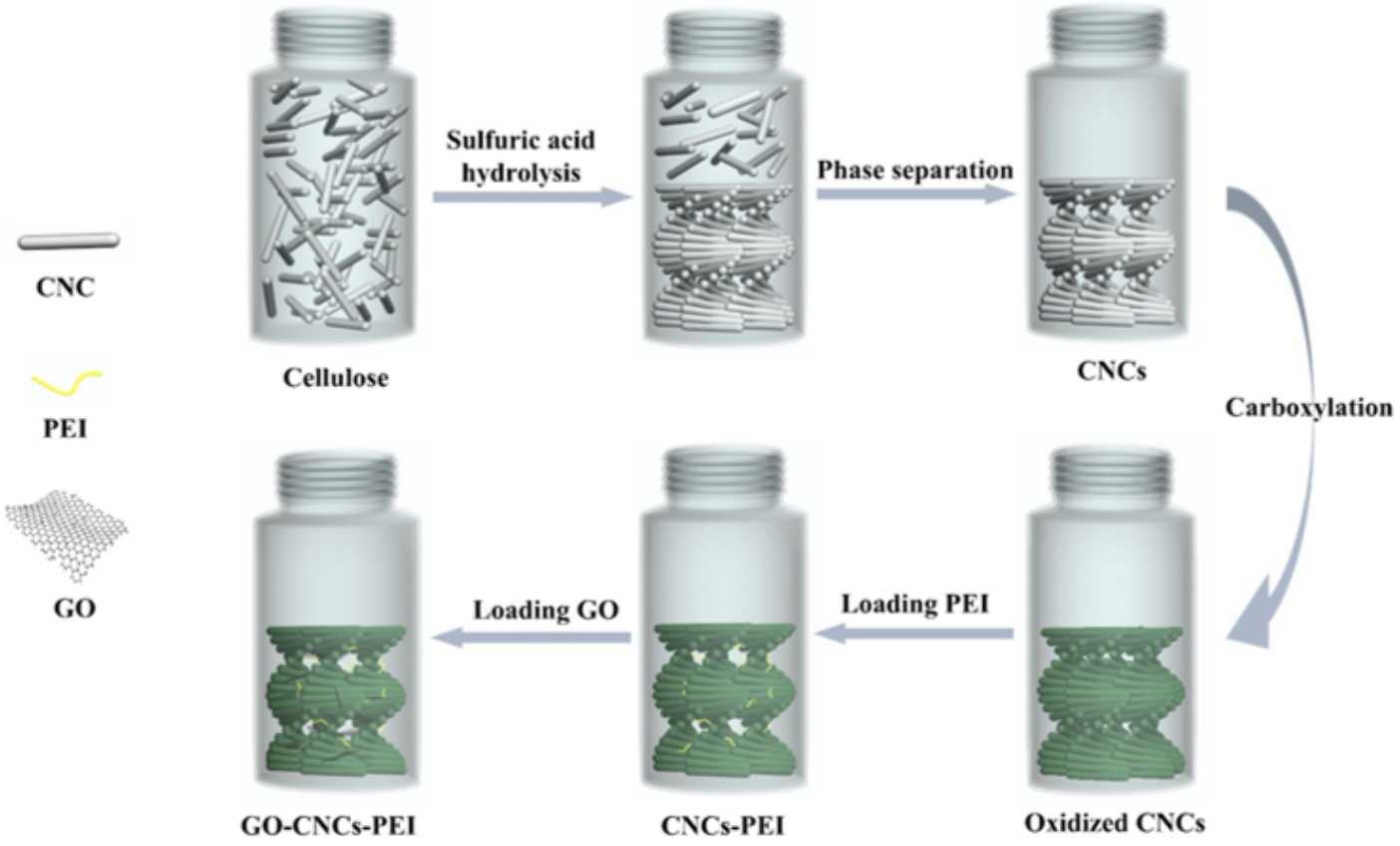

Figure 1

Synthesis of cellulose nanocrystals aerogel

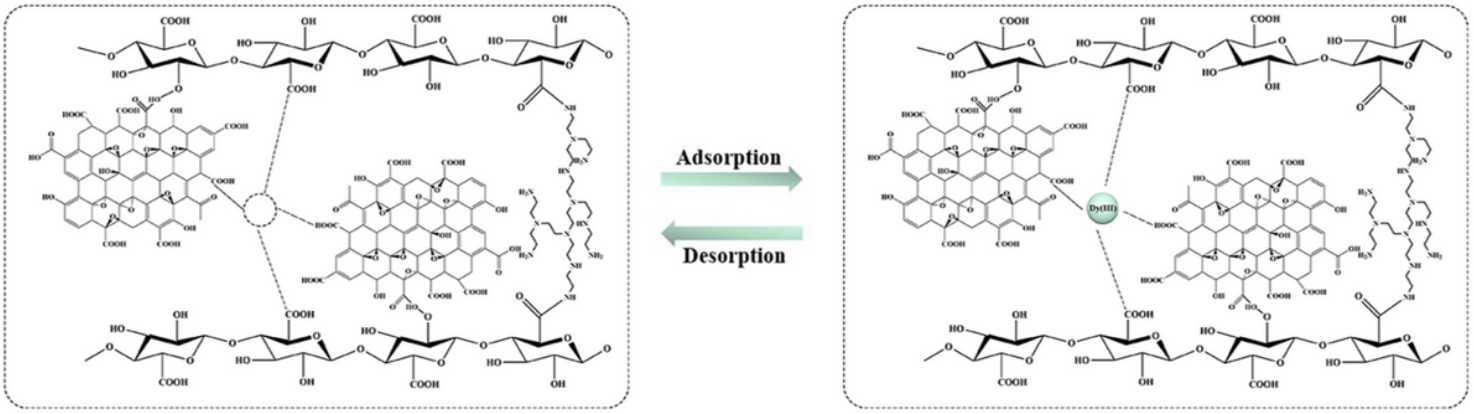

Figure 2

Possible adsorption mechanism for Dy(III) onto IGCPA.

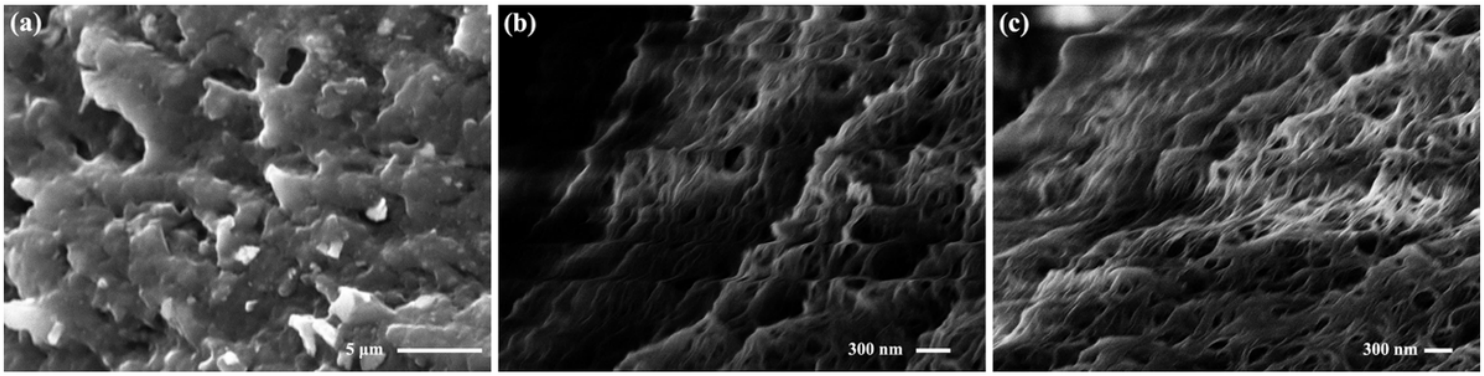

Figure 3

SEM images of PEI-CNCs aerogel (a), GCPA (b) and IGCPA(c).

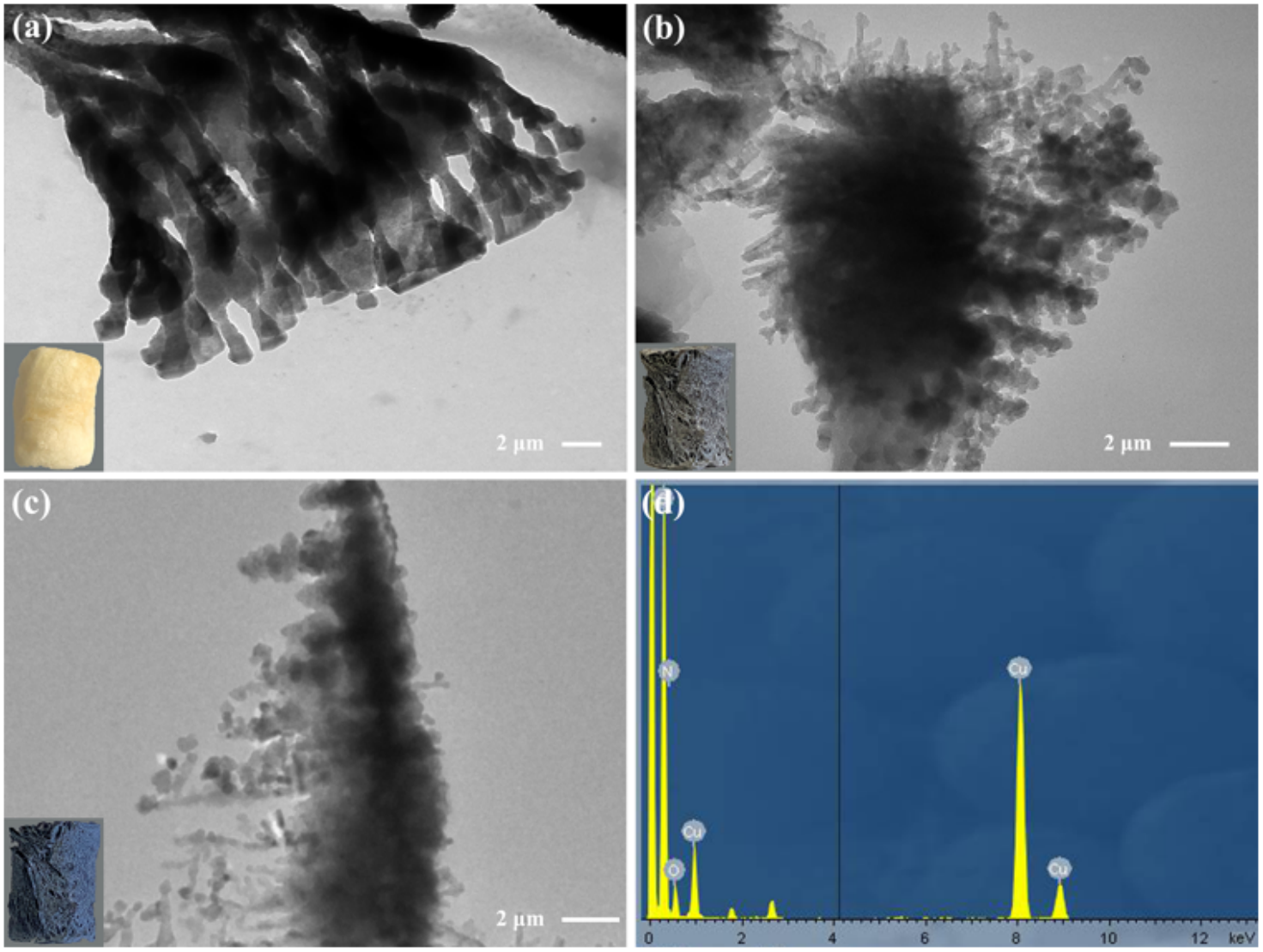

Figure 4

TEM images of PEI-CNCs aerogel (a), GCPA (b) and IGCPA (c), EDS element analysis of IGCPA (d).

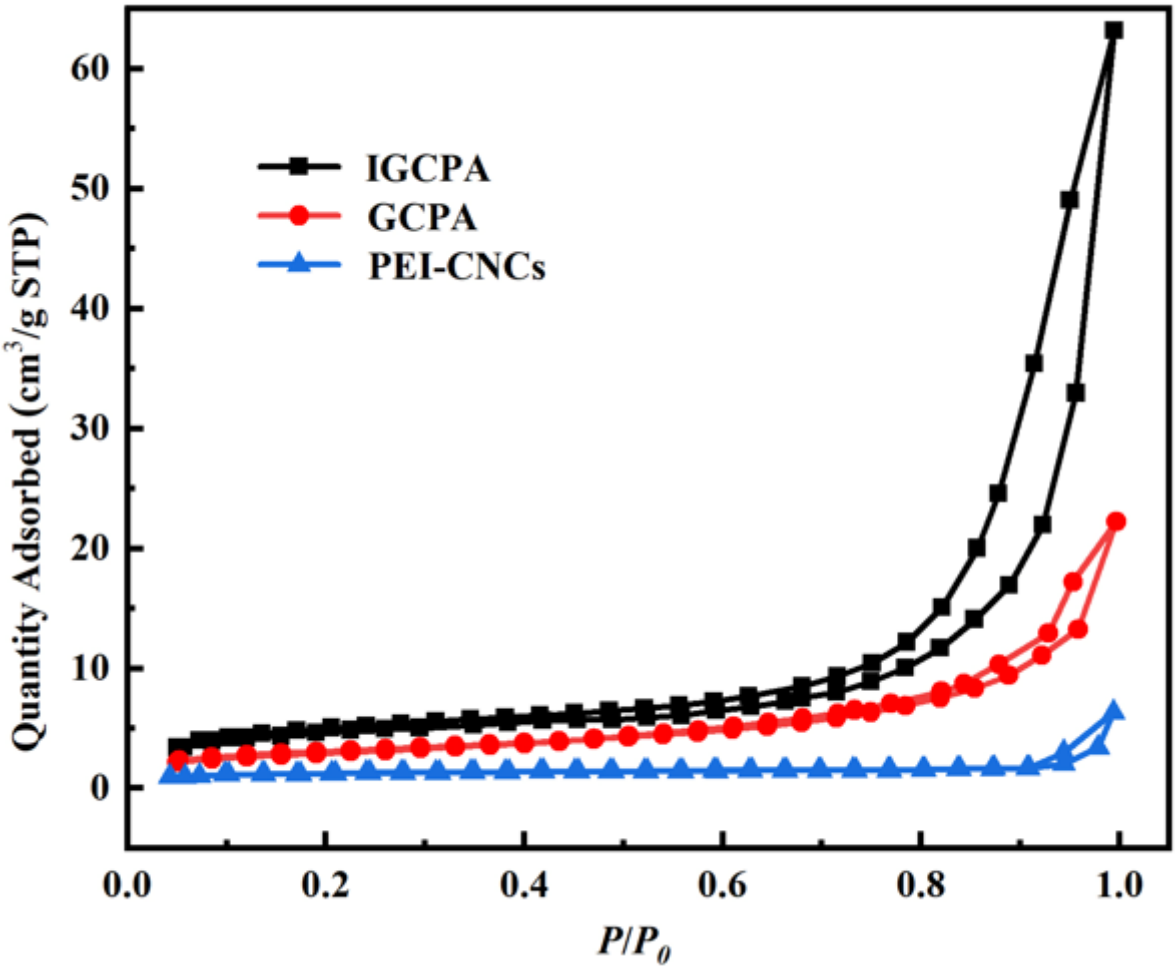

Figure 5

N2 adsorption-desorption isotherms of PEI-CNCs, GCPA and IGCPA.

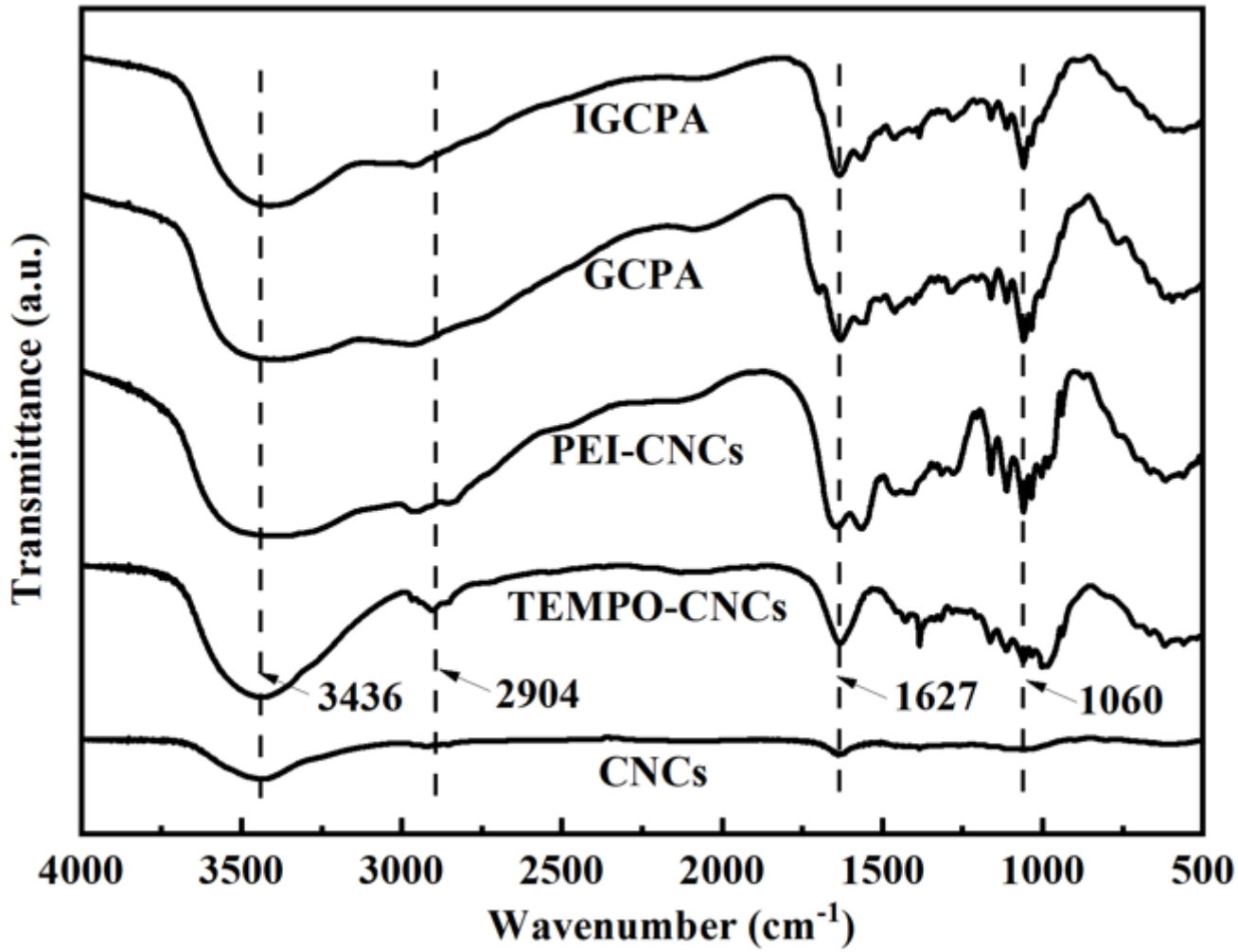

Figure 6

FT-IR spectra of aerogels.

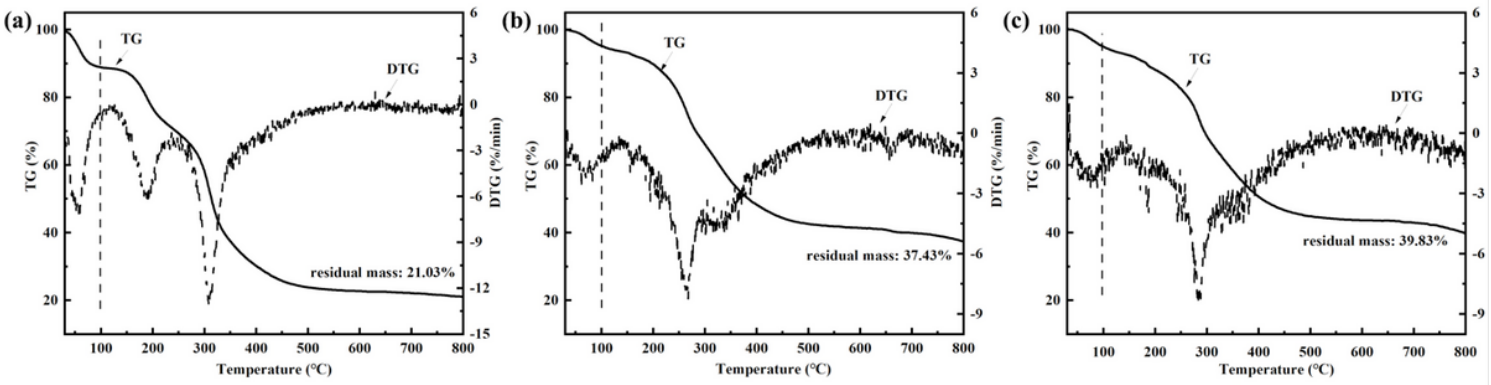

Figure 7

TGA curves of PEI-CNCs (a), GCPA (b) and IGCPA (c).

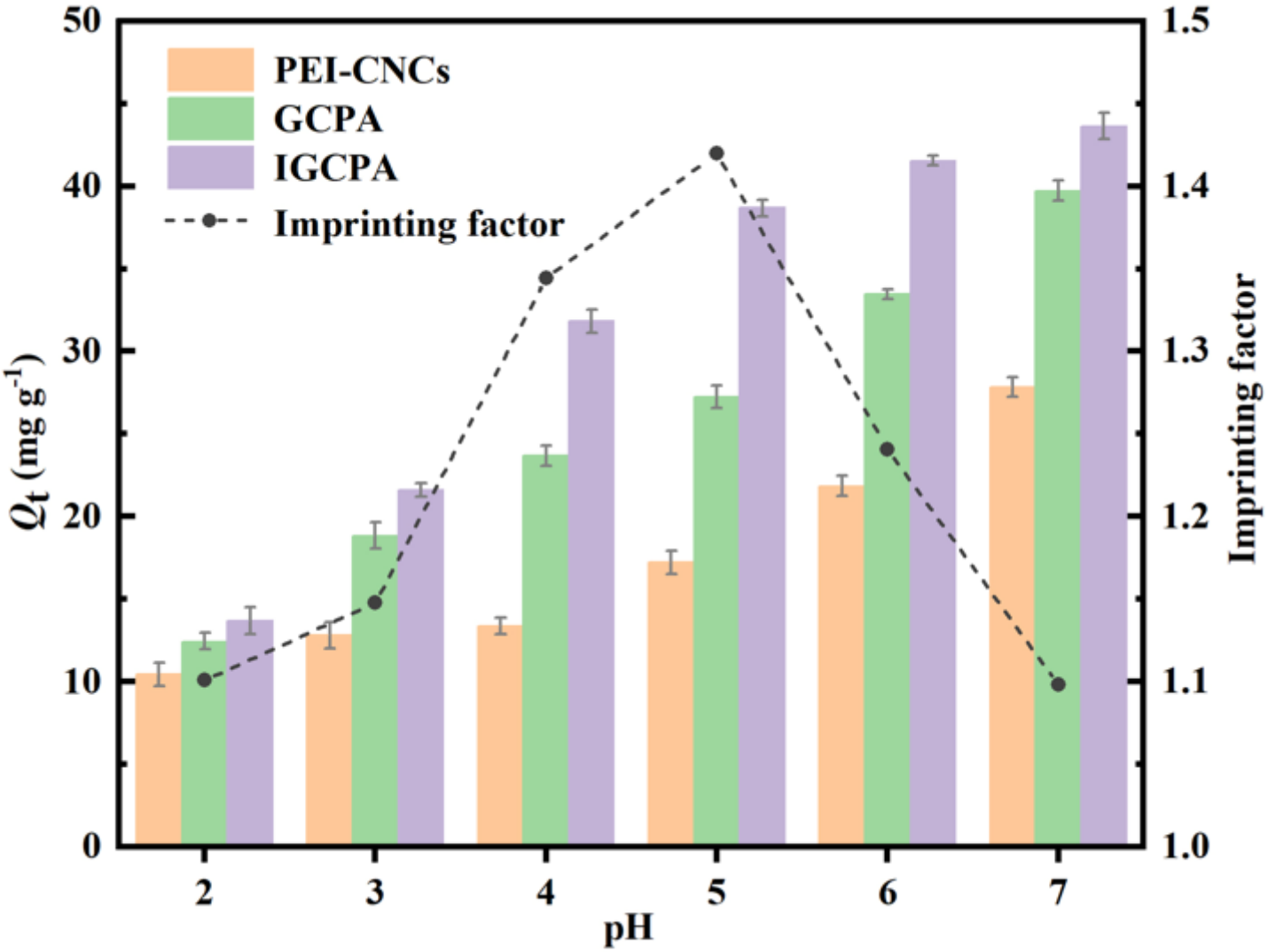

Figure 8

Effect of pH on the adsorption properties of PEI-CNCs, GCPA, IGCPA.

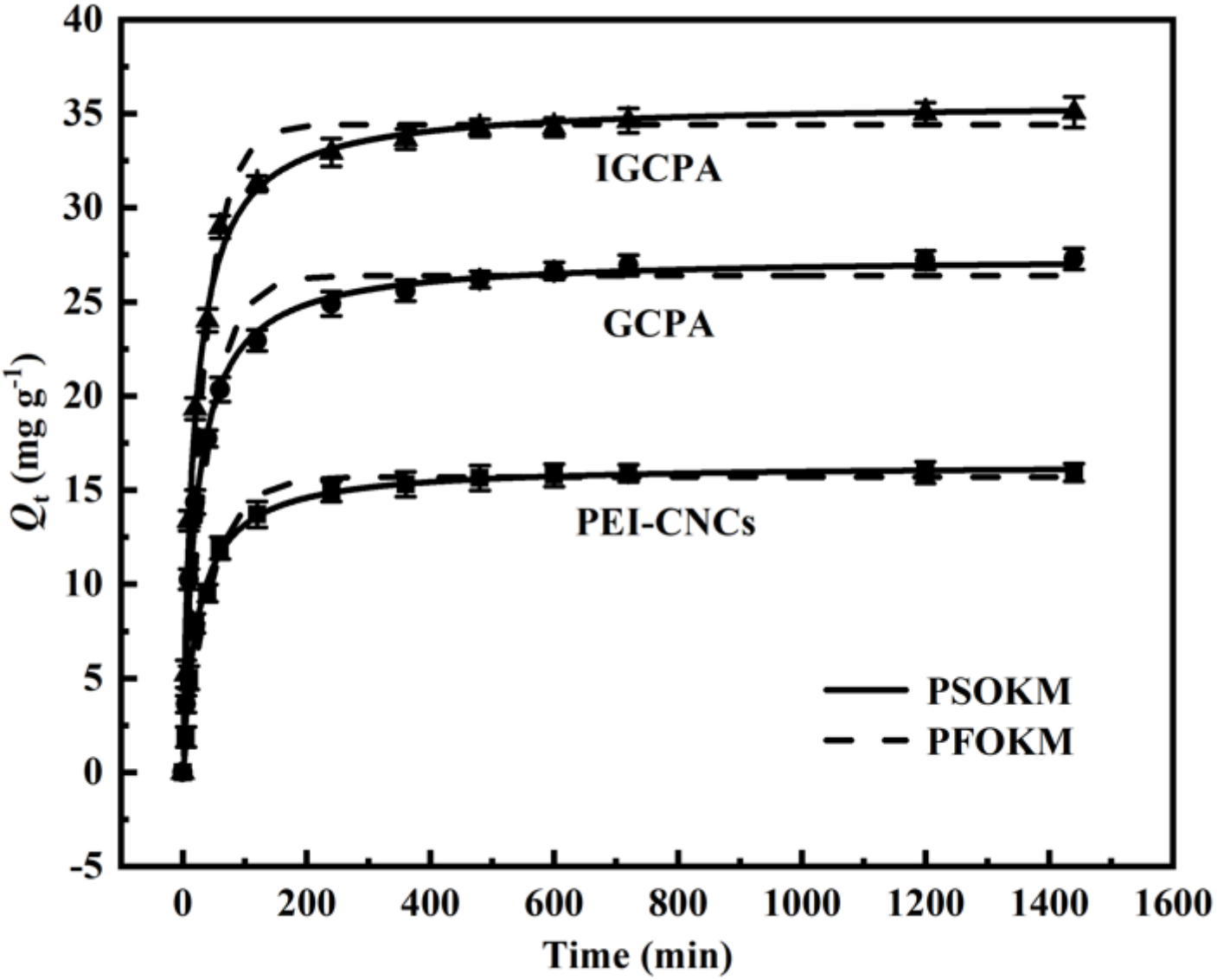

Figure 9

Kinetic data and modeling for the adsorption of Dy(III).

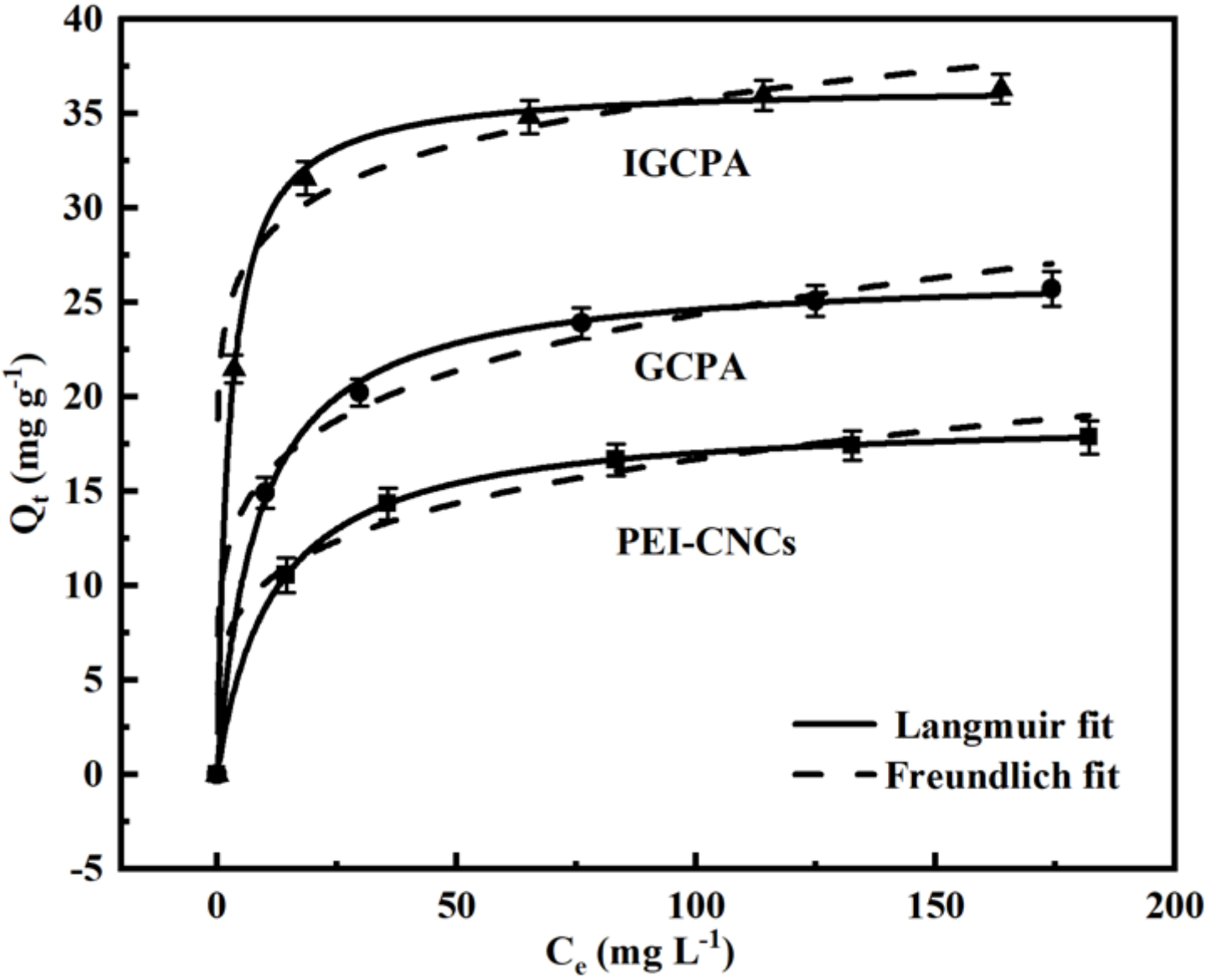

Figure 10

Adsorption isotherm of Dy(III) by aerogels.

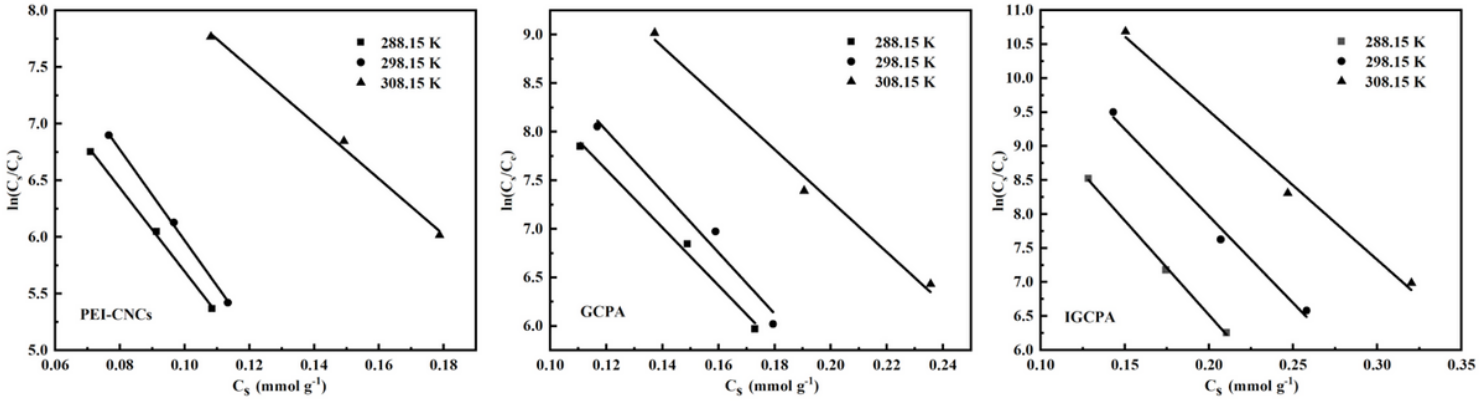

Figure 11

Thermodynamic properties of three aerogels at different temperatures: a plot of ln(Cs/Ce).

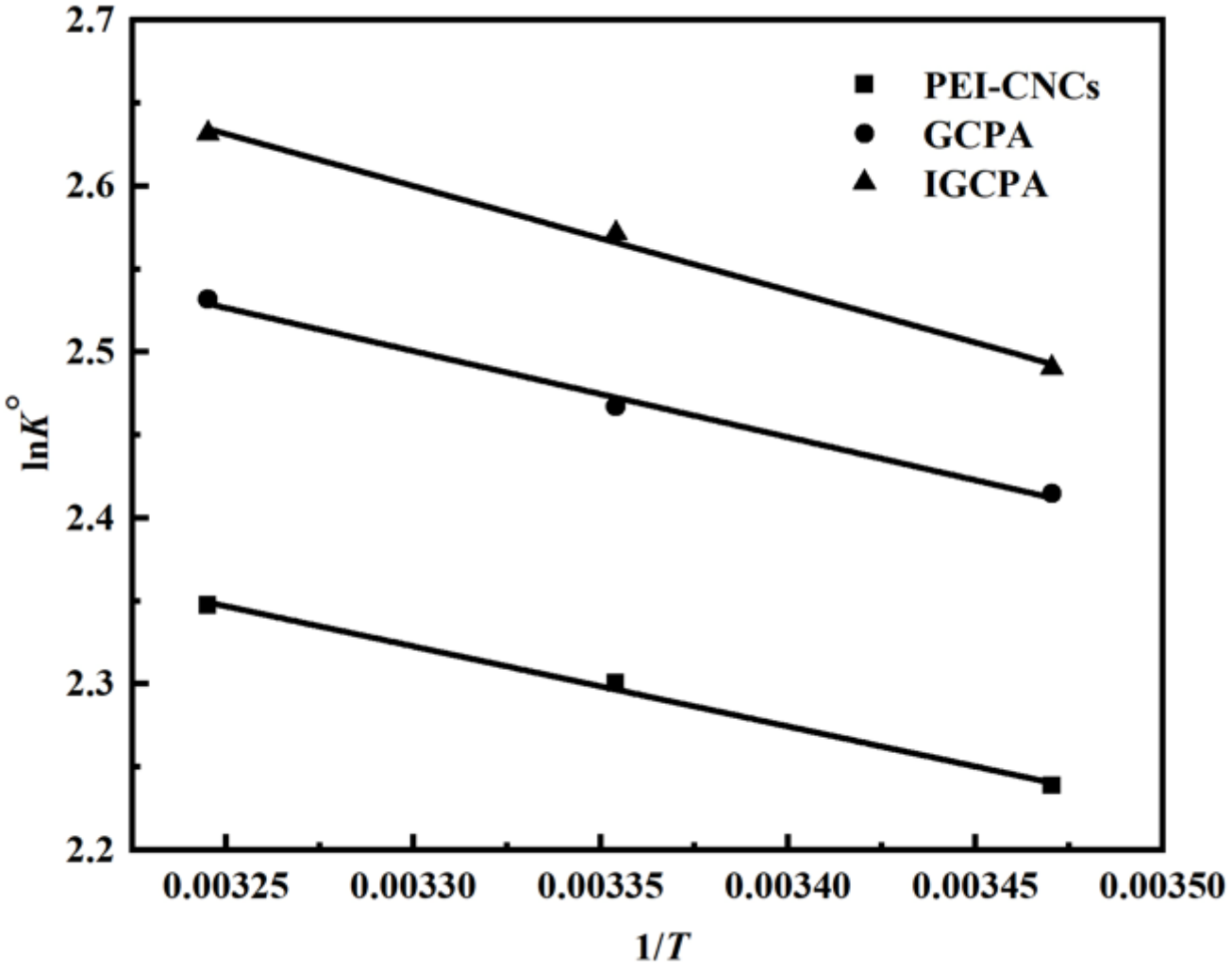

Figure 12

Thermodynamic properties of three aerogels at different temperatures: lnK° degrees versus 1/T.

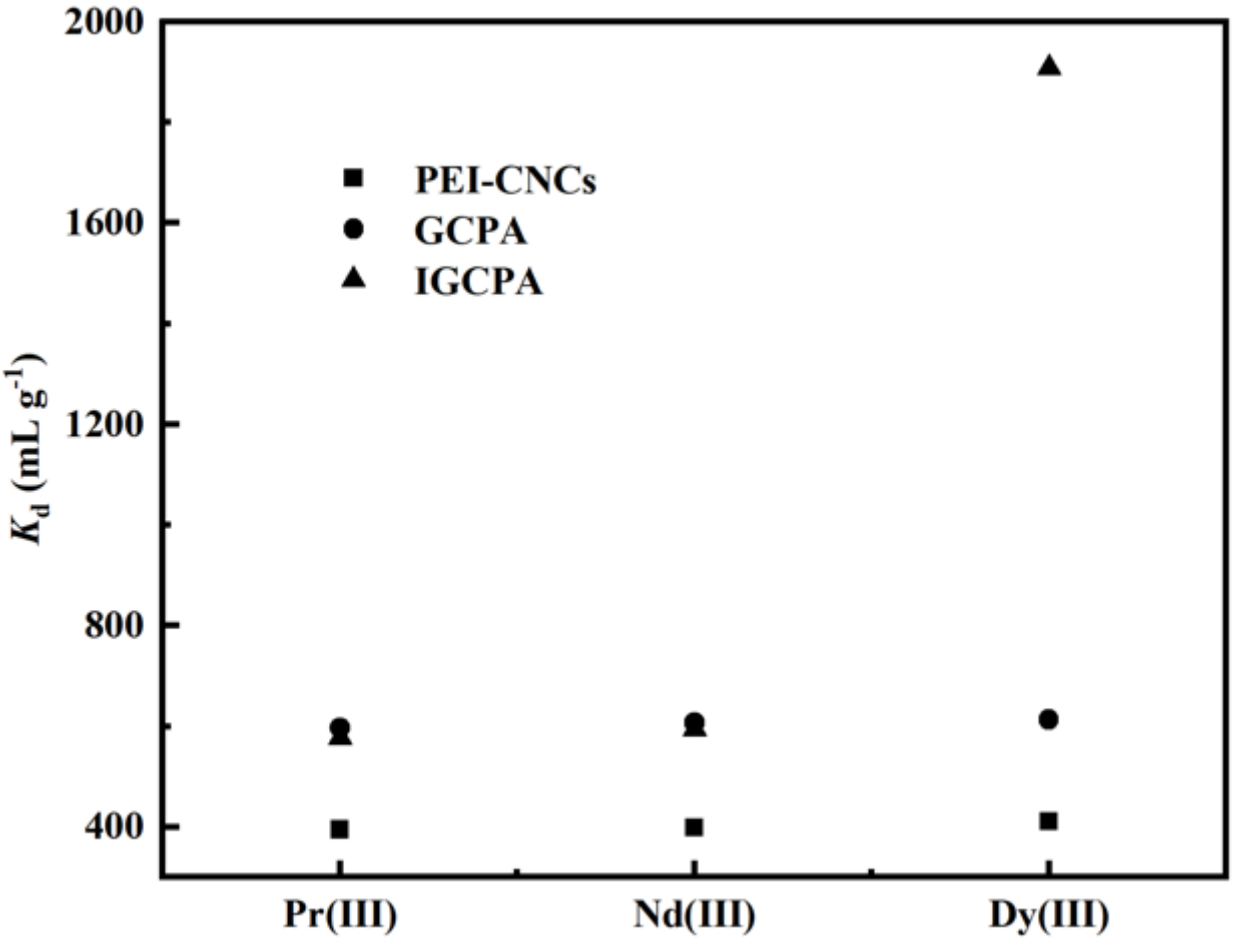

Figure 13

The Kd values of different ions adsorbed by aerogels.

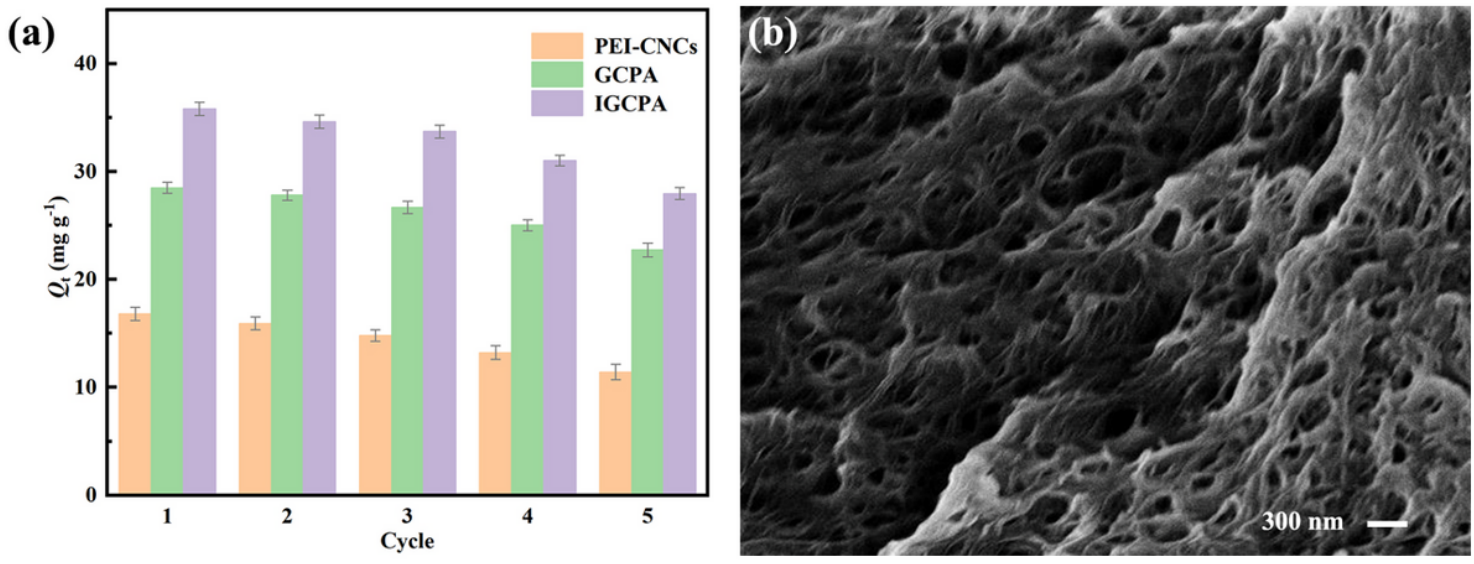

Figure 14

Regeneration of aerogels and the SEM image of IGCPA over 5 cycles.